THE JOURNAL OF BIOLOGICAL CHEMISTRY VOL. 290, NO. 10, pp. 6270–6280, March 6, 2015

Anoctamin-6 Controls Bone Mineralization by Activating the Calcium Transporter NCX1*[S]

Received for publication, August 11, 2014, and in revised form, January 13, 2015 Published, JBC Papers in Press, January 14, 2015, DOI 10.1074/jbc.M114.602979

Jiraporn Ousingsawat[‡], Podchanart Wanitchakool[‡], Rainer Schreiber[‡], Manuela Wuelling[§], Andrea Vortkamp[§], and Karl Kunzelmann[‡1]

From the [‡]Institut für Physiologie, Universität Regensburg, D-93053 Regensburg and the [§]Department Entwicklungsbiologie, Fakultät für Biologie, Universität Duisburg-Essen, 45141 Essen, Germany

Background: Deletion of Ano6 leads to reduced skeleton size and skeletal deformities.
Results: Ca^{2+}-activated anion currents are missing in primary osteoblasts from Ano6 null mice. Ano6 is required for the Na^+/Ca^{2+} exchanger NCX1 to operate in osteoblasts.
Conclusion: The Na^+/Ca^{2+} exchanger NCX1 is essential for bone mineralization and requires Ano6 to fully operate.
Significance: Ano6 supports NCX1, which is essential for bone mineralization.

Anoctamin-6 (Ano6, TMEM16F) belongs to a family of putative Ca^{2+}-activated Cl^- channels and operates as membrane phospholipid scramblase. Deletion of Ano6 leads to reduced skeleton size, skeletal deformities, and mineralization defects in mice. However, it remains entirely unclear how a lack of Ano6 leads to a delay in bone mineralization by osteoblasts. The Na^+/Ca^{2+} exchanger NCX1 was found to interact with Ano6 in a two-hybrid split-ubiquitin screen. Using human osteoblasts and osteoblasts from Ano6$^{-/-}$ and WT mice, we demonstrate that NCX1 requires Ano6 to efficiently translocate Ca^{2+} out of osteoblasts into the calcifying bone matrix. Ca^{2+}-activated anion currents are missing in primary osteoblasts isolated from Ano6 null mice. Our findings demonstrate the importance of NCX1 for bone mineralization and explain why deletion of an ion channel leads to the observed mineralization defect: Ano6 Cl^- currents are probably required to operate as a Cl^- bypass channel, thereby compensating net Na^+ charge movement by NCX1.

During vertebrate skeletal development, specialized cells, the osteoblasts, produce a mineralized bone matrix by deposition of hydroxyapatite crystals in the extracellular collagen matrix, where they become embedded and differentiate into osteocytes (1–3). This process requires the organized transport of high concentrations of Ca^{2+} and phosphate ions into the extracellular matrix without inducing premature crystallization. Although of fundamental importance, the process of calcification is not well understood. Different concepts currently exist. (i) A cell-independent mechanism has been suggested, whereby charged non-collagenous proteins associate with the collagen matrix to form mineralization foci (4). (ii) The amorphous calcium phosphate theory predicts that initial amorphous calcium phosphate is deposited, which gradually converts to pure crystalline hydroxyapatite (5, 6). (iii) A cell-controlled mechanism that requires budding of vesicles from the plasma membrane has also been proposed. These vesicles accumulate ions and organize the formation of calcium phosphate crystallization seeds containing hydroxyapatite particles. Subsequently, rupture of these vesicles spreads calcium phosphate onto the extracellular matrix (7, 8). (iv) Recent work identified intracellular vesicles that contain mineral in a mostly amorphous phase form (9, 10).

Whatever the precise mechanism is, mineralization requires Ca^{2+} transport. The mechanisms of Ca^{2+} transport by osteoblasts are not well understood at the molecular level. The Ca^{2+}-permeable transient receptor potential channels TRPV4 and TRPV6 are expressed in bone cells, but whether they affect bone mineralization has not yet been elucidated (11). Another group of Ca^{2+} transporters, the plasma membrane Ca^{2+}-ATPases, are strong candidates to transport Ca^{2+} into the extracellular compartment. PMCA1, PMCA2, and PMCA4 are expressed in osteoblasts, but their role in mineralization in mammals *in vivo* has not been demonstrated. In zebrafish, the PMCA2 homolog Atp2b1a seems to be required for mineralization by odontoblasts and possibly the adjacent bone structures (11–14). A third class of Ca^{2+} transporters are the Na^+/Ca^{2+} exchangers (NCX). Of these, NCX1 and NCX3 are expressed in mouse osteoblasts, and NCX3 has been demonstrated to regulate Ca^{2+} transport in osteoblastic cell lines (14–17).

Recently, anoctamin-6 (Ano6, TMEM16F) has been reported as another protein required for proper bone mineralization (1). Ano6 belongs to a family of putative Ca^{2+}-activated Cl^- channels (18–21). Several reports demonstrated that Ano6 generates an outwardly rectifying Cl^- current when activated by a large increase in local intracellular Ca^{2+} concentrations (22–24). Moreover, Ano6 operates as a Ca^{2+}-activated phospholipid scramblase that leads to movement of phosphatidylserine from the inner to the outer leaflet of the plasma membrane bilayer (25). Impaired Ca^{2+}-dependent phospholipid scrambling of phospholipids in platelets leads to Scott syndrome, a rare inherited defect in primary hemostasis due to mutations in

* This work was supported by Deutsche Forschungsgemeinschaft Grants DFG SFB699 (Project A7/A12) and DFG KU756/12-1.
[S] This article contains supplemental Tables 1 and 2.
[1] To whom correspondence should be addressed: Institut für Physiologie, Universität Regensburg, Universitätsstr. 31, D-93053 Regensburg, Germany. Tel.: 49-941-943-4302; Fax: 49-941-943-4315; E-mail: karl.kunzelmann@ur.de.

Ano6 (25, 26). The defect in Ca^{2+}-dependent phospholipid scrambling in cells from patients with Scott disease is paralleled by lack of Ca^{2+}-dependent activation of Cl^- currents, which is necessary for full platelet phosphatidylserine exposure and procoagulant activity (26, 27). Recently, reconstitution of a purified Ano6 homolog from *Aspergillus fumigatus* confirmed that Ano6 has both ion channel and scramblase function and that transport of both ions and lipids is controlled by a single Ca^{2+}-binding site (28).

A role of Ano6 in activating phosphatidylserine scrambling in osteoblasts has been demonstrated previously (1). However, its function as a Ca^{2+}-activated Cl^- channel has not been investigated in osteoblasts. In this study, we therefore examined the role of Ano6 Cl^- currents in the mineralization process. Notably, in a yeast two-hybrid split-ubiquitin screen using Ano6 as bait, we found the Na^+/Ca^{2+} exchanger NCX1 to be a potential binding partner, suggesting a molecular and functional link between Ano6 and NCX1.

EXPERIMENTAL PROCEDURES

Ano6-deficient Mice, RT-PCR, and Two-hybrid Analysis—Generation of Ano6 (TMEM16F)-deficient mice has been described (1). Total RNA was isolated from human and mouse osteoblasts using NucleoSpin RNA II columns (Macherey-Nagel GmbH & Co. KG, Düren, Germany). Total RNA (1 μg/50-μl reaction) was reverse-transcribed using random primers (Promega, Mannheim, Germany) and Moloney murine leukemia virus reverse transcriptase (RNase H Minus; Promega). Each RT-PCR contained sense and antisense primers for anoctamins (0.5 μM; see supplemental Tables 1 and 2) or for GAPDH (0.5 μM), 0.5 μl of cDNA, and GoTaq polymerase (Promega). After 2 min at 95 °C, cDNA was amplified in 30 cycles for 30 s at 95 °C, 30 s at 57 °C, and 1 min at 72 °C. PCR products were visualized by loading on ethidium bromide-containing agarose gels and analyzed using MetaMorph Version 6.2 (Molecular Devices). The two-hybrid split-ubiquitin screenings were performed using a normalized human universal NubG-x library with human Ano6 as a bait (Dualsystems Biotech AG, Zurich, Switzerland).

Primary Osteoblasts, Mineralization Assay, and HEK293 Cells—Frontal and parietal parts of mouse calvariae were dissected from day 18.5 embryos, and primary osteoblasts were isolated by two 30-min digestion steps in 0.1% collagenase IV (Sigma). Cells from individual animals were cultured separately, seeded at a density of 10^4 cells/cm^2, and cultured in DMEM supplemented with 10% fetal bovine serum and penicillin/streptomycin. Upon confluence, cells were reseeded at a density of 10^4 cells/cm^2 and cultured in the presence of 10 mM glycerophosphate and 5 mM ascorbate phosphate to induce osteogenic differentiation and mineralization (day 0). After establishing a nontoxic effective concentration, cells were treated with 5 μM tannic acid or KB-R7943 (29). The potential toxicity of these inhibitors was excluded by negative trypan blue staining and by assessing the effect of these inhibitors on cell morphology (data not shown). Moreover, previous *in vivo* and *in vitro* studies demonstrated the nontoxicity of these inhibitors (30–32).

TABLE 1
Potential partners for interaction with the Na^+/Ca^{2+} exchanger NCX1 as identified in a two-hybrid split-ubiquitin analysis
OS, organism name; GN, gene name; PE, protein existence; SV, sequence version.

UniProt ID	Protein
O60613	15-kDa selenoprotein
Q13686	Alkylated DNA repair protein
Q96GG9	DCN1-like protein 1
P06746	DNA polymerase β
Q9Y253	DNA polymerase η
P61978	Heterogeneous nuclear ribonucleoprotein KO
P01903	HLA class II histocompatibility antigen, DR α chain
P01033	Metalloproteinase inhibitor 1
P00912	*N*- (5′-Phosphoribosyl)anthranilate isomerase
P61758	Prefoldin subunit 3
O75934	Pre-mRNA-splicing factor SPF27
Q8IVG9	Putative humanin peptide
P32418	Sodium/calcium exchanger 1
P48643	T-complex protein 1 subunit ϵ
Q8N6G2	Testis-expressed sequence 26 protein
Q96B02	Ubiquitin-conjugating enzyme E2
Q9Y3C8	Ubiquitin-fold modifier-conjugating enzyme 1
Q8N6I4	UPF0694 transmembrane protein C14orf109
Q6UX73	UPF0764 protein C16orf89
Q9H0V9	VIP36-like protein
Q8WU90	Zinc finger CCCH domain-containing protein 15
P17028	Zinc finger protein 24
P08708	40 S ribosomal protein S17
Q9Y3U8	60 S ribosomal protein L36
P08548	LINE-1 reverse transcriptase homolog
P10451	Osteopontin
Q86U02	Putative uncharacterized protein C14orf165
Q8WTZ3	Zinc finger protein ENSP00000375192
P00846	ATP synthase subunit a
P00156	Cytochrome *b* (OS = *Homo sapiens*, GN = *MT-CYB*, PE = 1, SV = 1)
P00395	Cytochrome *c* oxidase subunit 1
P02792	Ferritin light chain
P03886	NADH-ubiquinone oxidoreductase chain 1
P03901	NADH-ubiquinone oxidoreductase chain 4L
P0CG47	Polyubiquitin-B (OS = *H. sapiens*, GN = *UBB*, PE = 1, SV = 1)
Q9Y6A9	Signal peptidase complex subunit 1

During differentiation, triplicate wells of each culture were fixed at days 3, 10, 17, and 20 in methanol and washed in deionized water. Staining intensity was quantified as described by Gregory *et al.* (33). Human primary osteoblasts were purchased from PromoCell (Heidelberg, Germany). Cells were grown in either osteoblast growth medium or osteoblast mineralization medium (PromoCell) according to the manufacturer's protocol. Mineralization was visualized by Alizarin Red staining, which was subsequently quantified (33). Briefly, Alizarin Red S was extracted from the cell layer in 10% acetic acid, and cell debris was removed by centrifugation and quantified at 405 nm in a microplate reader (NOVOstar, BMG LABTECH, Offenburg, Germany). HEK293 human embryonic kidney cells were grown in DMEM supplemented with 10% FBS. Cells were incubated in 5% CO_2 at 37 °C. pcDNA3.1 encoding human Ano6 and human NCX1 was transfected into HEK293 cells using standard methods (Lipofectamine, Invitrogen). Cells were examined 48 or 72 h after transfection.

Western Blotting of Ano6 in Human Primary Osteoblasts and Co-immunoprecipitation of NCX1/Ano6 in HEK293 Cells—Cells were collected and lysed in Nonidet P-40 lysis buffer (25 mM Tris-HCl (pH 7.4), 150 mM NaCl, 1 mM EDTA, 0.5% Nonidet P-40, 5% glycerol, and 1× protease inhibitor mixture). Proteins (20 μg) were analyzed by 10% SDS-PAGE and transferred

to PVDF membrane. The membrane was blocked with 5% non-fat milk in Tris-buffered saline containing 0.05% Tween 20 (NFM/TBST) for 1 h at room temperature and incubated overnight at 4 °C with rabbit anti-human Ano6 polyclonal antibody (diluted 1:500 in 1% NFM/TBST; P78, Davids Biotechnologie GmbH, Regensburg, Germany). Subsequently, the membrane was incubated with HRP-conjugated goat anti-rabbit IgG (diluted 1:10,000 in 1% NFM/TBST) for 2 h at room temperature. The immunoreactive signals were visualized using a SuperSignal chemiluminescence substrate detection kit (Pierce). To compare amounts of proteins, the membranes were probed with rabbit anti-β-actin antibody (diluted 1:1000 in 1% NFM/TBST; Sigma). The intensity of bands was quantified by densitometric scanning and normalized to β-actin.

Cell lysates in Nonidet P-40 lysis buffer were precleaned with protein G-agarose at 4 °C for 1 h. Cell lysates were incubated with 5 μg of primary antibody (goat anti-GFP or rabbit anti-NCX1 polyclonal antibody) overnight at 4 °C on a rotator. Cell lysates (70 μl containing 50 μg of protein) were incubated with protein G-agarose at 4 °C for 3 h, followed by centrifugation three times at 1000 × *g* for 1 min. Pellets were collected and resuspended in 1× loading buffer. The supernatant was collected, separated by 10% SDS-PAGE, and transferred to PVDF membrane. The membrane was blocked with 5% NFM/TBST for 1 h at room temperature and incubated overnight at 4 °C with goat anti-GFP polyclonal antibody (diluted 1:3000 in 1% NFM/TBST) or rabbit anti-NCX1 polyclonal antibody (diluted 1:1000 in 5% NFM/TBST). Subsequently, the membrane was incubated with HRP-conjugated donkey anti-goat IgG (diluted 1:2000 in 5% NFM/TBST) at room temperature for 1 h or with HRP-conjugated goat anti-rabbit IgG (diluted 1:10,000 in 1% NFM/TBST) at room temperature for 2 h. Immunoreactive signals were visualized using the SuperSignal chemiluminescence substrate detection kit.

Patch Clamping—Cells grown on coverslips were mounted in a perfused bath on the stage of a Zeiss IM35 inverted microscope and kept at 37 °C. The bath was perfused continuously with Ringer's solution (145 mM NaCl, 0.4 mM KH_2PO_4, 1.6 mM K_2HPO_4, 6 mM D-glucose, 1 mM $MgCl_2$, and 1.3 mM calcium gluconate (pH 7.4)) at ~10 ml/min. Patch clamp experiments were performed in the fast whole cell configuration. Patch pipettes had an input resistance of 4–6 megohms when filled with an intracellular-like solution containing 30 mM KCl, mM 95 potassium gluconate, 1.2 mM NaH_2PO_4, 4.8 mM Na_2HPO_4, 1 mM EGTA, 0.758 mM calcium gluconate, 1.034 mM $MgCl_2$, 5 mM D-glucose, and 3 mM ATP. The pH was 7.2, and the Ca^{2+} activity was 0.1 μM or 1 mM. The access conductance was measured continuously and was 90–140 nanosiemens (EPC-9 amplifier, List Medical Electronics, Darmstadt, Germany). In regular intervals, membrane voltages were clamped in steps of 20 mV from −100 to +100 mV from a holding potential of −60 mV.

Intracellular Ca^{2+} Concentrations in HEK293 Cells Coexpressing Ano6 and NCX1—Cells were seeded on glass coverslips and loaded with 2 μM Fura-2/AM and 0.02% Pluronic F-127 (Invitrogen) in Ringer's solution (145 mmol/liter NaCl, 0.4 mmol/liter KH_2PO_4, 1.6 mmol/liter K_2HPO_4, 5 mmol/liter glucose, 1 mmol/liter $MgCl_2$, and 1.3 mmol/liter calcium gluconate) for 1 h at room temperature. Fluorescence was detected

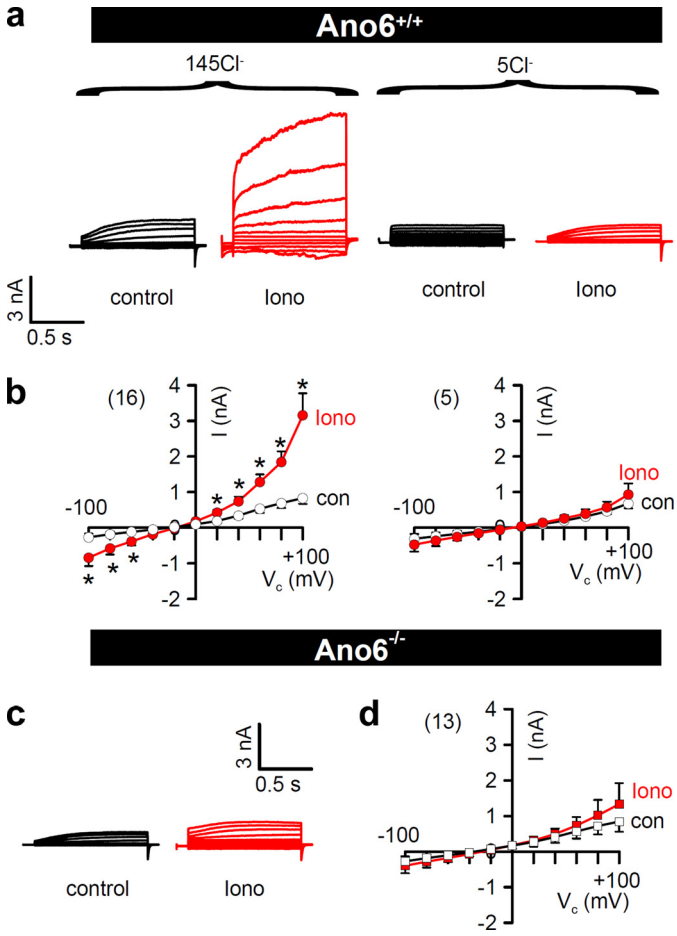

FIGURE 1. **Missing Ca^{2+}-activated whole cell currents in primary osteoblasts from Ano6$^{-/-}$ mice.** *a*, whole cell ion currents in WT osteoblasts (Ano6$^{+/+}$) measured under control conditions and after stimulation with the Ca^{2+} ionophore ionomycin (*Iono*; 1 μM). The holding voltage was −100 mV. The cells were voltage-clamped by ±100 mV in steps of 20 mV. Experiments were performed in the presence of 145 mM extracellular Cl^- (*145Cl$^-$*; *left*) or after replacement of 140 mM Cl^- with impermeable gluconate (*5Cl$^-$*; *right*). Removal of Cl^- ions inhibited whole cell currents, indicating activation of Cl^- currents by ionomycin. *b*, current/voltage relationships before (control (*con*)) and after stimulation with ionomycin in the presence of high (145 mM; *left*) or low (5 mM; *right*) extracellular Cl^-. V_c, voltage clamp. *c*, whole cell currents were not enhanced by ionomycin in knock-out osteoblasts (Ano6$^{-/-}$). *d*, corresponding current/voltage relationships before and after stimulation with ionomycin. Values represent mean ± S.E. *, significant increase by ionomycin (paired *t* test). The number of cells is indicated in *parentheses*.

in cells perfused with Ringer's solution at 37 °C using an inverted microscope (Axiovert S100, Zeiss) and a high speed polychromator system (VisiChrome, Puchheim, Germany). Fura-2 was excited at 340/380 nm, and emission was recorded between 470 and 550 nm using a CoolSNAP HQ camera (Visitron Systems). $[Ca^{2+}]_i$ was calculated from the 340/380 nm fluorescence ratio after background subtraction. The formula used to calculate $[Ca^{2+}]_i$ was as follows; $[Ca^{2+}]_i = K_d \times (R - R_{min})/(R_{max} - R) \times (S_{f2}/S_{b2})$, where R is the observed fluorescence ratio. The values R_{max} and R_{min} (maximum and minimum ratios) and the constant S_{f2}/S_{b2} (fluorescence of free and Ca^{2+}-bound Fura-2 at 380 nm) were calculated using 1 μM ionomycin (Calbiochem), 5 μM nigericin, 10 μM monensin (Sigma), and 5 mM EGTA to equilibrate intracellular and extracellular Ca^{2+} in intact Fura-2-loaded cells. The dissociation constant for the Fura-2·Ca^{2+} complex was taken as 224 nmol/

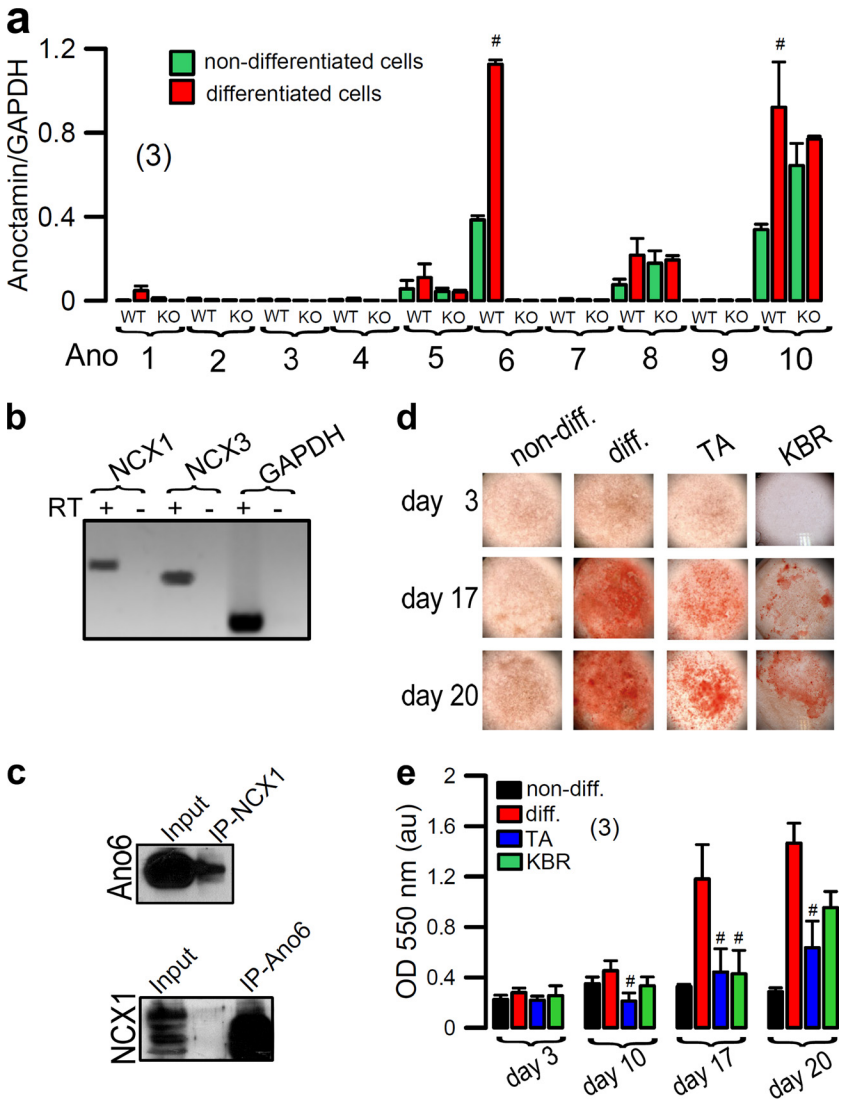

FIGURE 2. **Na^+/Ca^{2+} exchange and Cl^- transport through Ano6 are required for mineralization by mouse primary osteoblasts.** *a*, summary of RT-PCR analysis indicates up-regulation of Ano6 in differentiated WT osteoblasts and lack of expression of Ano6 in osteoblasts from Ano6$^{-/-}$ animals. *KO*, knock-out. *b*, RT-PCR analysis indicating expression of NCX1 and NCX3 in WT osteoblasts. *RT*, reverse transcriptase. *c*, co-immunoprecipitation of Ano6 with NCX1 (*upper panel*) and NCX1 with Ano6 (*lower panel*). 20 μg of lysate was loaded as an input control. No protein was pulled down when immunoprecipitation (*IP*) was done without antibody (beads only; $n = 6$ experiments). *d*, *in vitro* mineralization assays using Alizarin Red staining. Differentiated (*diff.*) *versus* non-differentiated (*non-diff.*) refers to the presence and absence, respectively, of β-glycerophosphate and ascorbate phosphate. Only differentiated osteoblasts demonstrated matrix mineralization. Mineralization was inhibited by KB-R7943 (*KBR*; 5 μM), indicating the contribution of Na^+/Ca^{2+} exchanger, and by the Ano6 blocker tannic acid (*TA*; 5 μM). All assays were performed in triplicates. *e*, optical density in shown arbitrary units (*au*). Values represent mean ± S.E. #, significantly different from non-differentiated cells (*a*) and differentiated cells (*e*) (analysis of variance).

liter. Experiments, imaging acquisition, and data analysis were controlled with the software packages MetaFluor (Molecular Devices) and Origin (OriginLab Corp.).

Materials and Statistics—All compounds used were the highest grade from Sigma (ionomycin, cyclopiazonic acid, tannic acid, KB-R7943, and CaCCinh-A01) or Merck. Student's *t* test (for paired or unpaired samples as appropriate) was used for statistical analysis. A p value <0.05 was accepted as significant.

RESULTS

Ca^{2+}-dependent Ion Currents and Mineralization by Mouse Primary Osteoblasts Require Ano6 and NCX—In two-hybrid split-ubiquitin screenings of a normalized human universal NubG-x library with human Ano6 as bait, we identified NCX1 as a potential Ano6-interacting protein. Although two-hybrid screening identified a number of potential Ano6 targets, NCX1 appeared most interesting (Table 1). We further analyzed the potential interaction partner NCX1 because Ano6-deficient mice have been shown to suffer from a bone mineralization defect, whereas NCX1 has been reported previously to control bone mineralization (1, 34). Moreover, Ano6 has been shown to form a Ca^{2+} channel (35) or may alternatively control Ca^{2+} transport through NCX1. Further evidence for a possible direct coupling of NCX1 and Ano6 was provided by co-immunoprecipitation of both proteins (see Fig. 2*c*). We hypothesized that both Ano6 and NCX1 may be required for Ca^{2+} transport by osteoblasts. To test if Ano6 and NCX1 are coexpressed in primary osteoblasts, cells were isolated from WT and Ano6$^{-/-}$ mice and grown in the presence of β-glycerophosphate and

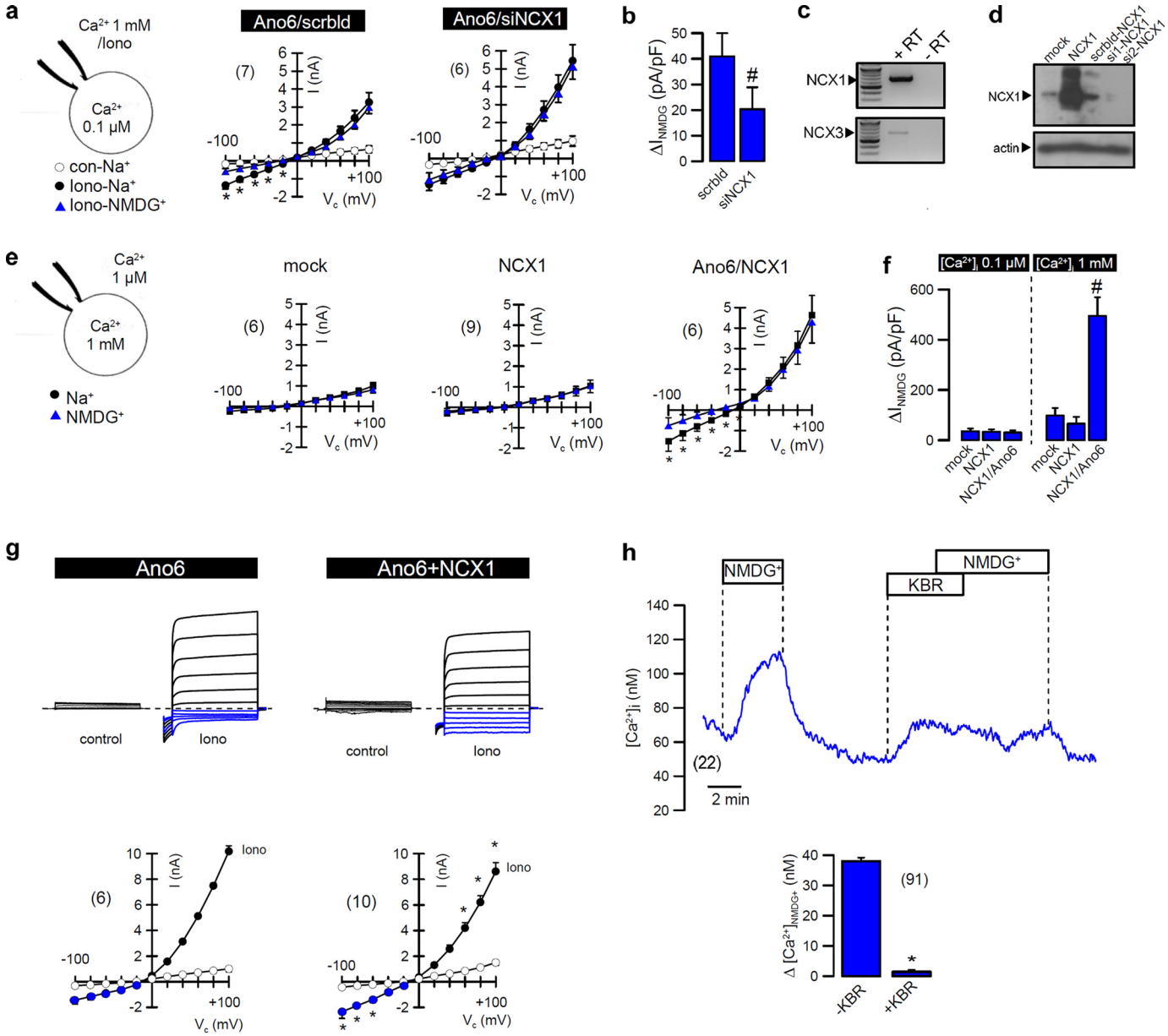

FIGURE 3. **Ano6 activates the Na^+/Ca^{2+} exchanger in HEK293 cells.** *a*, current/voltage relationships from whole cell patch clamp experiments in Ano6-expressing cells. Ionomycin (*Iono*; 1 μM)-activated currents were enhanced after knockdown of NCX1. *I/V* curves are shown after replacement of extracellular Na^+ with $NMDG^+$ (*blue triangles*). *con*, control. *b*, $NMDG^+$-sensitive inward currents (ΔI_{NMDG} at voltage clamp (V_c) of −100 mV) were reduced after knockdown of NCX1. *siNCX1*, NCX1 siRNA. *c*, RT-PCR analysis shows dominant expression of NCX1 in HEK293 cells. *RT*, reverse transcriptase. *d*, Western blot of NCX1 in cells transfected with empty plasmid (*mock*) or NCX1 or treated with scrambled RNA (*scrbld*) or siRNAs for NCX1. *e*, recordings with high (1 mM) Ca^{2+} in the patch pipette. Replacement of extracellular Na^+ with $NMDG^+$ blocked inward currents. *f*, $NMDG^+$-sensitive inward currents were detected only after coexpression of Ano6 and activation by high Ca^{2+}. Values represent mean ± S.E. #, significant effect of $NMDG^+$ (unpaired *t* test). *g*, coexpression of NCX1 augments inward currents and reduces outward currents. *h*, *upper panel*, summary trace of cytosolic Ca^{2+} concentration that was enhanced by removal of extracellular Na^+ ($NMDG^+$) or inhibition of NCX1 by 10 μM KB-R7943 (*KBR*). *Lower panel*, summary of the $NMDG^+$-induced increase in intracellular Ca^{2+} in the absence or presence of KB-R7943. Values represent mean ± S.E. The number of cells is indicated in *parentheses*. *, significant effects of $NMDG^+$ or KB-R7943 (paired *t* test); #, significant difference compared with scrambled RNA or low Ca^{2+} (0.1 μM; unpaired *t* test). Blots were performed in triplicates.

ascorbate phosphate to induce osteogenic differentiation. By RT-PCR, we observed expression of Ano6, Ano8, and Ano10 in WT osteoblasts. Expression of Ano6 and Ano10 was up-regulated during differentiation (see Fig. 2*a*). No Ano6 mRNA was detected in osteoblasts from $Ano6^{-/-}$ animals (see Fig. 2*a*) (1). We found that an increase in $[Ca^{2+}]_i$ by the Ca^{2+} ionophore ionomycin activated Cl^- currents only in WT (but not $Ano6^{-/-}$) osteoblasts (Fig. 1). Apart from Ano6, also Na^+/Ca^{2+} exchangers (NCX1 and NCX3) were expressed in primary osteoblasts (Fig. 2*b*). Using Alizarin Red staining, we detected prominent mineralization at days 17 and 20 of mouse primary calvarial cultures (Fig. 2*d*). Mineralization was delayed after treatment of these osteoblasts with the NCX inhibitor KB-R7943, supporting a role of Na^+/Ca^{2+} exchange in the mineralization process (36). Mineralization was also significantly inhibited by the Ano6 inhibitor tannic acid (30), demonstrating the role of Ano6 Cl^- currents in mineralization.

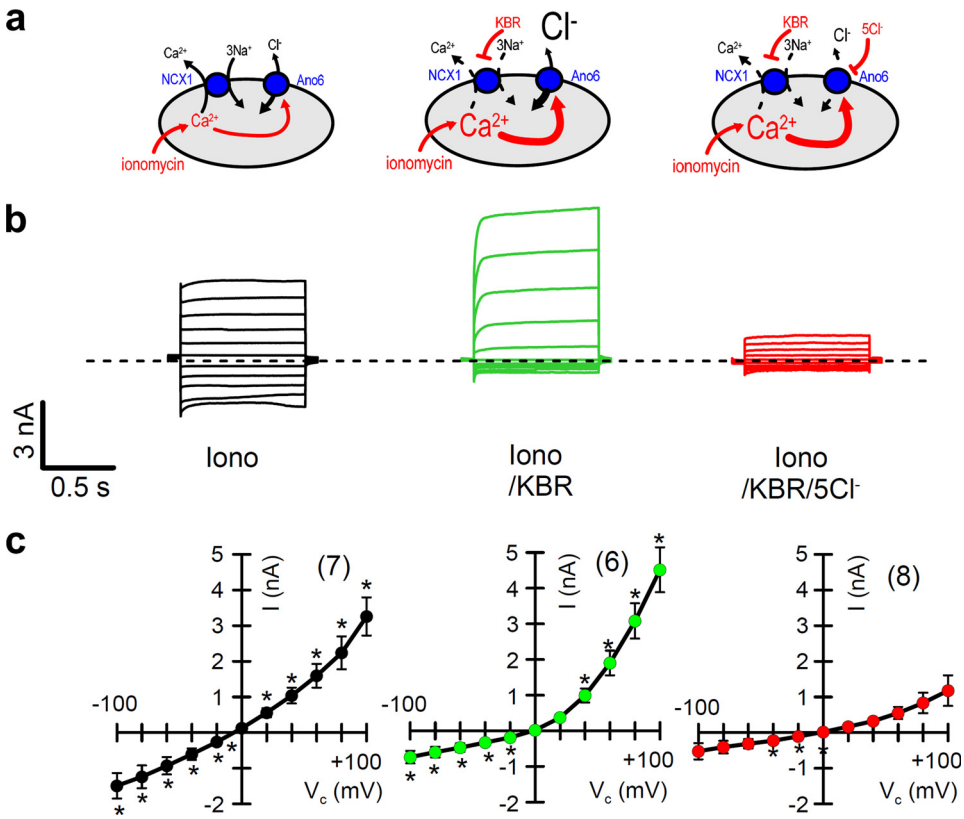

FIGURE 4. **Parallel transport by Ano6 and NCX1.** *a*, schematic illustrating intracellular Ca^{2+} levels under various conditions. *b*, whole cell overlay currents activated by ionomycin (*Iono*) in HEK293 cells coexpressing Ano6 and NCX1 (holding voltage of −100 mV, steps of 20 mV, ±100 mV). Currents are shown under control conditions, in the presence of 10 μM KB-R7943 (*KBR*), and after replacement of extracellular Cl^- with gluconate (*5Cl*$^-$). *c*, summary of current/voltage relationships for the conditions as shown above. Values represent mean ± S.E. *, significant increase by ionomycin (paired *t* test). The number of cells is indicated in *parentheses*. V_c, voltage clamp.

Ano6 Drives the Forward Mode of the Na^+/Ca^{2+} Exchanger—We further examined the functional relationship between Ano6 and NCX1 in HEK293 cells (14). An increase in $[Ca^{2+}]_i$ by ionomycin activated whole cell Cl^- currents in HEK293 cells overexpressing Ano6 (Fig. 3*a*) (22). We observed a small negative (Na^+ inward) current that was inhibited when extracellular Na^+ was replaced with impermeable *N*-methyl-D-glucamine ($NMDG^+$).[2] We suggested that the $NMDG^+$-sensitive inward current is due to electrogenic transport by the Na^+/Ca^{2+} exchanger NCX1 (Fig. 3, *a* and *b*). Endogenous expression of NCX1 in HEK293 cells was effectively knocked down by siRNA (Fig. 3, *c* and *d*). Inhibition of NCX1 expression attenuated $NMDG^+$-sensitive Na^+ inward currents and augmented Cl^- outward currents. Thus, ionomycin-induced increase in $[Ca^{2+}]_i$ appears to be larger in the absence of Na^+ or after reduced expression of NCX1. Measurements of intracellular Ca^{2+} demonstrated that inhibition of NCX1 by $NMDG^+$ augmented $[Ca^{2+}]_i$ (Fig. 3*h*, *upper panel*). In the presence of extracellular $NMDG^+$, NCX1 operated in the reverse mode, thus transporting Ca^{2+} into the cell. Blocking NCX1 with KB-R7943 inhibited Ca^{2+} outward transport; therefore, the Ca^{2+} increase was less pronounced. Notably, $NMDG^+$ had no effects on $[Ca^{2+}]_i$ in the presence of the NCX1 blocker KB-R7943 (Fig. 3*h*, *lower panel*).

Ion transport was also activated in NCX1/Ano6-expressing cells with high Ca^{2+} concentrations (1 mmol/liter) in the patch pipette. Notably, $NMDG^+$-inhibitable Na^+ currents (NCX1) were detected only in the presence of Ano6 (Fig. 3, *e* and *f*). Finally, when Ano6 and NCX1 were coexpressed, ionomycin-activated inward currents were larger, whereas outward currents were smaller compared with cells expressing only Ano6 (Fig. 3*g*). In contrast, inward currents decreased and outward currents increased after inhibition of NCX1 by KB-R7943 (Fig. 4). Both inward and outward currents were abolished by further removal of extracellular Cl^- ($5Cl^-$). These results indicate that Cl^- transport through Ano6 is essential for NCX1 to operate in the forward mode, *i.e.* to transport Ca^{2+} out of the cell.

Ano6 Supports Outward Transport of Ca^{2+} through the Na^+/Ca^{2+} Exchanger—We further demonstrated regulation of NCX1 by Ano6 in $[Ca^{2+}]_i$ measurements using Fura-2. Endoplasmic reticulum Ca^{2+} stores were emptied by cyclopiazonic acid in Ca^{2+}-free bath solution (Fig. 5*a*, *upper right scheme*). Re-addition of extracellular Ca^{2+} increased $[Ca^{2+}]_i$ only transiently through store-operated Ca^{2+} influx because Ca^{2+} was transported out of the cell by NCX1 $[Ca^{2+}]_i$. NCX1 was inhibited by KB-R7943, Na^+ replacement with $NMDG^+$, or inhibition of Ano6 currents by removal of extracellular Cl^- ($5Cl^-$)

[2] The abbreviations used are: $NMDG^+$, *N*-methyl-D-glucamine; CFTR, cystic fibrosis transmembrane conductance regulator.

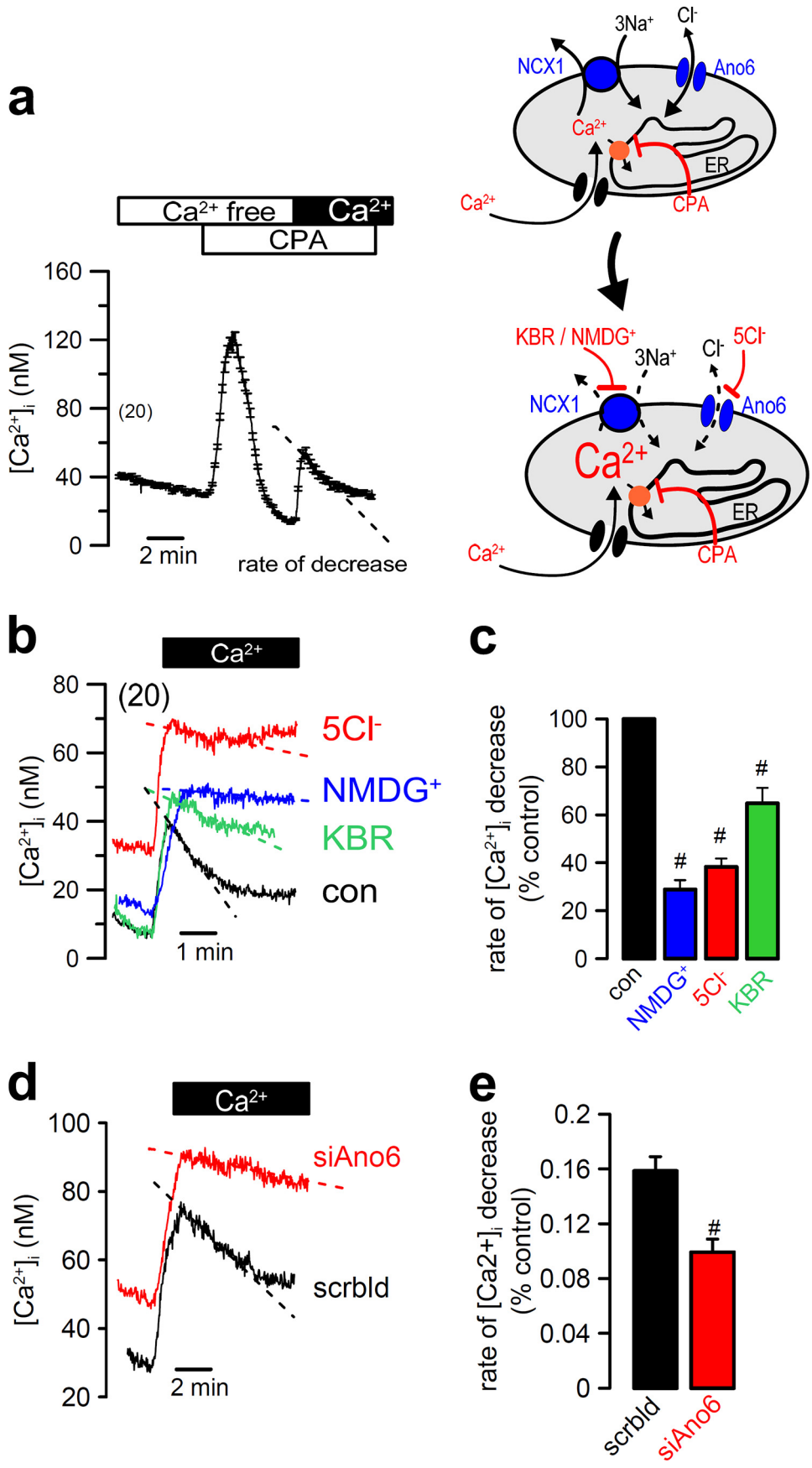
a
Ca2+ free
Ca2+
CPA
160
120
80
40
0
[Ca2+]i (nM)
(20)
2 min
rate of decrease
3Na+
Cl-
NCX1
Ano6
Ca2+
ER
CPA
KBR / NMDG+
5Cl-
b
Ca2+
(20)
5Cl-
NMDG+
KBR
con
1 min
c
rate of [Ca2+]i decrease (% control)
100
80
60
40
20
0
#
con
NMDG+
5Cl-
KBR
d
Ca2+
siAno6
scrbld
2 min
e
0.2
0.16
0.12
0.08
0.04
0
scrbld
siAno6

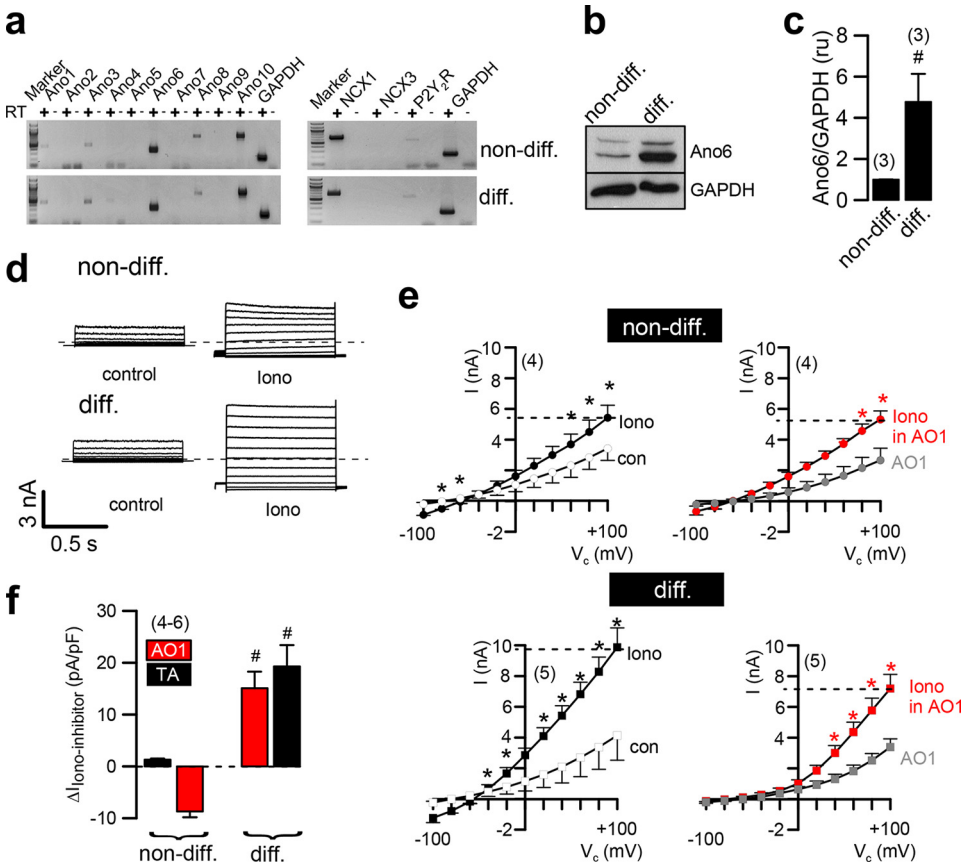

FIGURE 6. **Ca^{2+}-activated Ano6 Cl^- currents in primary human osteoblasts.** *a*, RT-PCR analysis indicates predominant expression of Ano6 and Ano10, as well as the Na^+/Ca^{2+} exchanger NCX1, in human primary osteoblasts. *b* and *c*, Western blots indicating up-regulation of Ano6 in differentiated osteoblasts (day 20 after treatment with glycerophosphate and ascorbate phosphate). *d*, whole cell overlay currents from non-differentiated (*non-diff.*) and differentiated (*diff.*) osteoblasts (holding voltage of −100 mV, steps of 20 mV, ±100 mV). *e*, current/voltage relationships obtained in non-differentiated (*upper panels*) and differentiated (*lower panels*) osteoblasts. Cells were stimulated with ionomycin (*Iono*; 1 μM) in the absence (*left panels*) or presence (*right panels*) of the anoctamin inhibitor CaCCinh-A01 (*AO1*; 10 μM). Inhibition of ionomycin-activated currents by CaCCinh-A01 was more pronounced in differentiated cells. *con*, control; V_c, voltage clamp. *f*, density of CaCCinh-A01- and tannic acid (*TA*)-sensitive currents in non-differentiated and differentiated osteoblasts. Values represent mean ± S.E. #, significant difference compared with non-differentiated cells (unpaired *t* test); *, significant increase by ionomycin (paired *t* test). The number of cells is indicated in *parentheses*. *pF*, picofarads.

(Fig. 5, *a* (*lower right scheme*), *b*, and c). Moreover, siRNA knockdown of Ano6 also inhibited outward transport of Ca^{2+} (Fig. 5, *d* and *e*). The results demonstrate the essential role of NCX1/Ano6 in controlling $[Ca^{2+}]_i$ in mouse osteoblasts and HEK293 cells.

Ano6 Supports Ca^{2+} Transport and Mineralization in Primary Human Osteoblasts—Mouse primary osteoblasts up-regulated Ano6 upon differentiation by β-glycerophosphate and ascorbate phosphate (Fig. 2*a*). Similar results were found in human primary osteoblasts. Human primary osteoblasts expressed predominately Ano6 and Ano10, with Ano6 being strongly up-regulated during differentiation (Fig. 6, *a–c*). An increase in intracellular Ca^{2+} by ionomycin activated whole cell currents, which were larger in differentiated cells. Similar, CaCCinh-A01-sensitive Cl^- currents were enhanced in differentiated cells (Fig. 6, *d–f*). These results suggest that similar to recombinant NCX1, also in mouse and human osteoblasts, NCX1 might be regulated by Ano6. We performed a mineralization assay in differentiated primary human osteoblasts, which demonstrated extracellular calcium phosphate deposition (Fig. 7*a*). Extracellular precipitation made patch clamp experiments often difficult because it limited the access of the patch pipette to the cell membrane. Similar to mouse osteoblasts, also in human osteoblasts, mineralization was strongly inhibited by inhibition of NCX1 with KB-R7943 or blocking of Ano6 with tannic acid (Fig. 7). The fact that blocking NCX1 reduced mineralization less than inhibition of Ano6 suggests additional Ca^{2+} export mechanisms unrelated to NCX1. Nevertheless, the data indicate that functional coupling of Ano6 and NCX1 is essential for bone min-

FIGURE 5. **Ano6 supports outward transport of Ca^{2+} through the Na^+/Ca^{2+} exchanger.** *a*, time course (mean ± S.E.) of $[Ca^{2+}]_i$ in HEK293 cells. Shown are the emptying of Ca^{2+} stores with 10 μM cyclopiazonic acid (*CPA*) in Ca^{2+}-free bath solution, the re-increase in $[Ca^{2+}]_i$ by Ca^{2+} influx in Ca^{2+}-containing buffer, and the subsequent decrease by the Na^+/Ca^{2+} exchanger NCX1 (*dashed line*). Schemes show transport activities and action of drugs. *ER*, endoplasmic reticulum. *b* and *c*, decrease in $[Ca^{2+}]_i$ in the absence or presence of NCX inhibitors (KB-R7943 (*KBR*), 10 μM), replacement of extracellular Na^+ with $NMDG^+$, and replacement of extracellular Cl^- with gluconate (*5Cl*$^-$). *d* and *e*, decrease in $[Ca^{2+}]_i$ in cells treated with scrambled RNA (*scrbld*) or Ano6 siRNA (*siAno6*). Values represent mean ± S.E. #, significant difference compared with the control (*con*) or scrambled RNA (unpaired *t* test). The number of cells is indicated in *parentheses*.

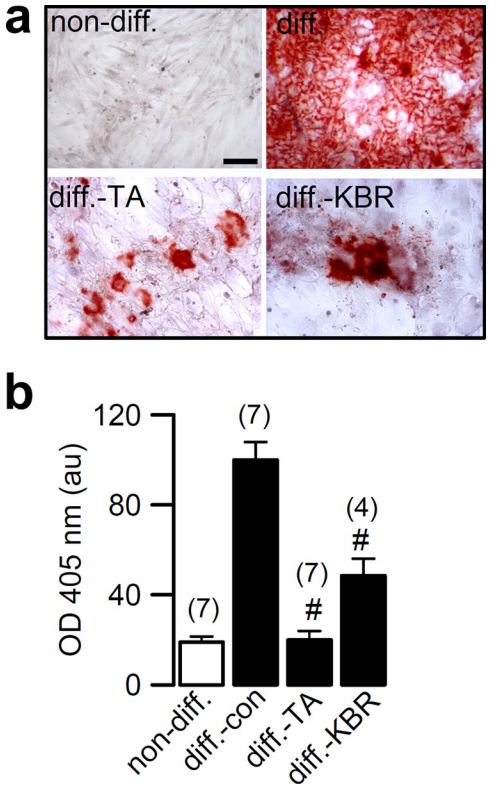

FIGURE 7. **Na^+/Ca^{2+} exchange and Cl^- transport through Ano6 are required for mineralization by primary human osteoblasts.** *a*, visualization of mineralization by primary human osteoblasts *in vitro* at day 20 of differentiated (*diff.*) cell culture using Alizarin Red staining. No mineralization was observed in non-differentiated (*non-diff.*) cells. Both tannic acid (*TA*; 10 μM; inhibition of Ano6) and KB-R7943 (*KB*; 10 μM; inhibition of Na^+/Ca^{2+} exchanger) inhibited mineralization. *Scale bar* = 20 μm. *b*, summary of Alizarin Red assays indicating significant increase in mineralization in differentiated cells inhibited by TA and KB-R7943. The optical density in shown in arbitrary units (*au*). Values represent mean ± S.E. #, significant difference (unpaired *t* test). The number of assays are indicated in *parentheses*.

eralization, which explains the skeletal defect observed in Ano6 null mice (Fig. 8).

DISCUSSION

Our results indicate that decreased mineral deposition in the skeletons of Ano6 null mice (1) is at least in part due to defective regulation of plasma membrane Na^+/Ca^{2+} exchange. Cl^- transport by Ano6 drives Ca^{2+} transport by NCX1, as indicated by inhibitors of Ano6 (CaCCinh-A01 and tannic acid), or removal of extracellular Cl^-. All inhibited deposition of hydroxyapatite by osteoblasts. We propose a model in which the Cl^- channel function of Ano6 serves to activate NCX1 and possibly NCX3, thereby increasing extracellular Ca^{2+} deposition, which is required for formation of hydroxyapatite in the extracellular matrix. As NCX1- or NCX2-deficient mice have not yet been reported, it is difficult to estimate if other Ca^{2+} transporters are also regulated by Ano6. Likewise, other anion channels may be linked to Ca^{2+} secretion. It is noteworthy that the cystic fibrosis transmembrane conductance regulator (CFTR) Cl^- channel is expressed in osteoblasts and in ameloblasts/odontoblasts (37). Cystic fibrosis patients carrying the common F508del mutation in the CFTR gene and mice carrying an inactivated CFTR allele suffer from bone mineralization

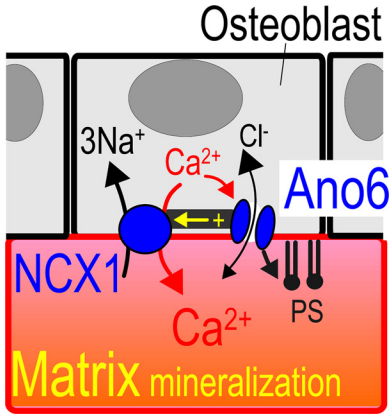

FIGURE 8. **Role of Ano6 and NCX1 in bone mineralization.** Shown is a schematic model of the roles of Ano6 and NCX1 in bone mineralization. Ca^{2+} increases in osteoblasts activate outwardly rectifying Ano6 Cl^- currents and the outward transport of Ca^{2+} by the Na^+/Ca^{2+} exchanger NCX1. The inward transport of Cl^- compensates the cytosolic positive transport potential by the electrogenic Na^+/Ca^{2+} exchanger, thereby maintaining Ca^{2+} outward transport at a high rate. NCX1 may directly interact with Ano6 (*yellow arrow*). Scrambling of phosphatidylserine (*PS*; *green*) by Ano6 supports the mineralization process.

defects leading to osteoporosis and osteopenia (37–40). The mechanisms of how CFTR operates in osteoblasts are only poorly understood. Nevertheless, the reduced bone mineral density underlines the importance of Cl^- transport in osteoblasts for proper bone formation.

Ano6-dependent Na^+/Ca^{2+} transport may also be related to the nonselective cation conductance that has been reported for Ano6 (35). We propose that instead of directly transporting Ca^{2+} ions, Ano6 may support the activity of the Na^+/Ca^{2+} exchanger.

The function of Ano6 in osteoblasts is reminiscent of the function of Ano1 in proximal tubular epithelial cells of the kidney (41). In the proximal tubule, protons are secreted by the vacuolar proton pump (V-ATPase). Translocation of H^+ to the tubular lumen by the Ca^{2+}-activated V-ATPase is an electrogenic process, and accumulation of charge may limit the transport activity of the pump. Parallel activation of Ano1 leads to Cl^- efflux that counterbalances charge movement, thereby facilitating H^+ secretion (41).

The mineralization defect in Ano6-deficient mice has previously been discussed as being linked to the scramblase function of Ano6, which is significantly impaired in osteoblasts (1). Here, we have shown that Ano6 facilitates matrix mineralization by supporting the function of the Na^+/Ca^{2+} exchanger (Fig. 8). However, the present data do not elucidate whether Na^+/Ca^{2+} exchangers operate to directly transport Ca^{2+} into the extracellular collagen matrix, where it gradually converts to crystalline hydroxyapatite (5), or whether Na^+/Ca^{2+} exchange takes place in budding vesicles or in intracellular calcium phosphate-containing vesicles (8–10). In this respect, it is of interest that exposure of phosphatidylserine has been proposed to be required for the formation of matrix vesicles and/or the localization of these vesicles to the collagen network (2). Ano6 might thus couple two essential functions: Ca^{2+} secretion and formation of matrix vesicles (Fig. 8).

Acknowledgments—We thank Daniel Auerbach and Nicolas Lentze (Dualsystems Biotech) for performing the two-hybrid split-ubiquitin analysis.

Note Added in Proof—Figs. 2c and 6*a* were not formatted correctly in the version of this article that was published on-line on January 14, 2015, as a Paper in Press. These figures have been revised to conform with JBC policies.

REFERENCES

1. Ehlen, H. W., Chinenkova, M., Moser, M., Munter, H. M., Krause, Y., Gross, S., Brachvogel, B., Wuelling, M., Kornak, U., and Vortkamp, A. (2013) Inactivation of anoctamin-6/Tmem16f, a regulator of phosphatidylserine scrambling in osteoblasts, leads to decreased mineral deposition in skeletal tissues. *J. Bone Miner. Res.* **28,** 246–259
2. Rosenberg, N., Rosenberg, O., and Soudry, M. (2012) Osteoblasts in bone physiology–mini review. *Rambam Maimonides Med. J.* **3,** e0013
3. Kornak, U. (2011) Animal models with pathological mineralization phenotypes. *Joint Bone Spine* **78,** 561–567
4. Glimcher, M. J. (1984) Recent studies of the mineral phase in bone and its possible linkage to the organic matrix by protein-bound phosphate bonds. *Philos. Trans. R. Soc. Lond. B Biol. Sci.* **304,** 479–508
5. Mahamid, J., Sharir, A., Addadi, L., and Weiner, S. (2008) Amorphous calcium phosphate is a major component of the forming fin bones of zebrafish: indications for an amorphous precursor phase. *Proc. Natl. Acad. Sci. U.S.A.* **105,** 12748–12753
6. Boskey, A. L. (1998) Biomineralization: conflicts, challenges, and opportunities. *J. Cell. Biochem. Suppl.* **30–31,** 83–91
7. Bonucci, E. (2009) Calcification and silicification: a comparative survey of the early stages of biomineralization. *J. Bone Miner. Metab.* **27,** 255–264
8. Anderson, H. C. (1995) Molecular biology of matrix vesicles. *Clin. Orthop. Relat. Res.* **314,** 266–280
9. Boonrungsiman, S., Gentleman, E., Carzaniga, R., Evans, N. D., McComb, D. W., Porter, A. E., and Stevens, M. M. (2012) The role of intracellular calcium phosphate in osteoblast-mediated bone apatite formation. *Proc. Natl. Acad. Sci. U.S.A.* **109,** 14170–14175
10. Mahamid, J., Sharir, A., Gur, D., Zelzer, E., Addadi, L., and Weiner, S. (2011) Bone mineralization proceeds through intracellular calcium phosphate loaded vesicles: a cryo-electron microscopy study. *J. Struct. Biol.* **174,** 527–535
11. van der Eerden, B. C., Weissgerber, P., Fratzl-Zelman, N., Olausson, J., Hoenderop, J. G., Schreuders-Koedam, M., Eijken, M., Roschger, P., de Vries, T. J., Chiba, H., Klaushofer, K., Flockerzi, V., Bindels, R. J., Freichel, M., and van Leeuwen, J. P. (2012) The transient receptor potential channel TRPV6 is dynamically expressed in bone cells but is not crucial for bone mineralization in mice. *J. Cell. Physiol.* **227,** 1951–1959
12. Go, W., and Korzh, V. (2013) Plasma membrane Ca^{2+} ATPase Atp2b1a regulates bone mineralization in zebrafish. *Bone* **54,** 48–57
13. Francis, M. J., Lees, R. L., Trujillo, E., Martín-Vasallo, P., Heersche, J. N., and Mobasheri, A. (2002) ATPase pumps in osteoclasts and osteoblasts. *Int. J. Biochem. Cell Biol.* **34,** 459–476
14. Li, J. P., Kajiya, H., Okamoto, F., Nakao, A., Iwamoto, T., and Okabe, K. (2007) Three Na^+/Ca^{2+} exchanger (NCX) variants are expressed in mouse osteoclasts and mediate calcium transport during bone resorption. *Endocrinology* **148,** 2116–2125
15. Linck, B., Qiu, Z., He, Z., Tong, Q., Hilgemann, D. W., and Philipson, K. D. (1998) Functional comparison of the three isoforms of the Na^+/Ca^{2+} exchanger (NCX1, NCX2, NCX3). *Am. J. Physiol.* **274,** C415–C423
16. Sosnoski, D. M., and Gay, C. V. (2008) NCX3 is a major functional isoform of the sodium-calcium exchanger in osteoblasts. *J. Cell. Biochem.* **103,** 1101–1110
17. Stains, J. P., Weber, J. A., and Gay, C. V. (2002) Expression of Na^+/Ca^{2+} exchanger isoforms (NCX1 and NCX3) and plasma membrane Ca^{2+} ATPase during osteoblast differentiation. *J. Cell. Biochem.* **84,** 625–635
18. Kunzelmann, K., Nilius, B., Owsianik, G., Schreiber, R., Ousingsawat, J., Sirianant, L., Wanitchakool, P., Bevers, E. M., and Heemskerk, J. W. (2014) Molecular functions of anoctamin 6 (TMEM16F): a chloride channel, cation channel or phospholipid scramblase? *Pflügers Arch.* **466,** 407–414
19. Yang, Y. D., Cho, H., Koo, J. Y., Tak, M. H., Cho, Y., Shim, W. S., Park, S. P., Lee, J., Lee, B., Kim, B. M., Raouf, R., Shin, Y. K., and Oh, U. (2008) TMEM16A confers receptor-activated calcium-dependent chloride conductance. *Nature* **455,** 1210–1215
20. Schroeder, B. C., Cheng, T., Jan, Y. N., and Jan, L. Y. (2008) Expression cloning of TMEM16A as a calcium-activated chloride channel subunit. *Cell* **134,** 1019–1029
21. Caputo, A., Caci, E., Ferrera, L., Pedemonte, N., Barsanti, C., Sondo, E., Pfeffer, U., Ravazzolo, R., Zegarra-Moran, O., and Galietta, L. J. (2008) TMEM16A, a membrane protein associated with calcium-dependent chloride channel activity. *Science* **322,** 590–594
22. Tian, Y., Schreiber, R., and Kunzelmann, K. (2012) Anoctamins are a family of Ca^{2+} activated Cl^- channels. *J. Cell Sci.* **125,** 4991–4998
23. Grubb, S., Poulsen, K. A., Juul, C. A., Kyed, T., Klausen, T. K., Larsen, E. H., and Hoffmann, E. K. (2013) TMEM16F (anoctamin 6), an anion channel of delayed Ca^{2+} activation. *J Gen. Physiol.* **141,** 585–600
24. Shimizu, T., Iehara, T., Sato, K., Fujii, T., Sakai, H., and Okada, Y. (2013) TMEM16F is a component of a Ca^{2+}-activated Cl^- channel but not a volume-sensitive outwardly rectifying Cl^- channel. *Am. J. Physiol. Cell Physiol.* **304,** C748–C759
25. Suzuki, J., Umeda, M., Sims, P. J., and Nagata, S. (2010) Calcium-dependent phospholipid scrambling by TMEM16F. *Nature* **468,** 834–838
26. Kmit, A., van Kruchten, R., Ousingsawat, J., Mattheij, N. J., Senden-Gijsbers, B., Heemskerk, J. W., Schreiber, R., Bevers, E. M., and Kunzelmann, K. (2013) Calcium-activated and apoptotic phospholipid scrambling induced by Ano6 can occur independently of Ano6 ion currents. *Cell Death Dis.* **4,** e611
27. Harper, M. T., and Poole, A. W. (2013) Chloride channels are necessary for full platelet phosphatidylserine exposure and procoagulant activity. *Cell Death. Dis.* **4,** e969
28. Malvezzi, M., Chalat, M., Janjusevic, R., Picollo, A., Terashima, H., Menon, A. K., and Accardi, A. (2013) Ca^{2+}-dependent phospholipid scrambling by a reconstituted TMEM16 ion channel. *Nat. Commun.* **4,** 2367
29. Lundquist, P., Lundgren, T., Gritli-Linde, A., and Linde, A. (2000) Na^+/Ca^{2+} exchanger isoforms of rat odontoblasts and osteoblasts. *Calcif. Tissue Int.* **67,** 60–67
30. Namkung, W., Thiagarajah, J. R., Phuan, P. W., and Verkman, A. S. (2010) Inhibition of Ca^{2+}-activated Cl^- channels by gallotannins as a possible molecular basis for health benefits of red wine and green tea. *FASEB J.* **24,** 4178–4186
31. Namkung, W., Phuan, P. W., and Verkman, A. S. (2011) TMEM16A inhibitors reveal TMEM16A as a minor component of calcium-activated chloride channel conductance in airway and intestinal epithelial cells. *J. Biol. Chem.* **286,** 2365–2374
32. Ludewig, U., Pusch, M., and Jentsch, T. J. (1996) Two physically distinct pores in the dimeric ClC-0 chloride channel. *Nature* **383,** 340–343
33. Gregory, C. A., Gunn, W. G., Peister, A., and Prockop, D. J. (2004) An Alizarin red-based assay of mineralization by adherent cells in culture: comparison with cetylpyridinium chloride extraction. *Anal. Biochem.* **329,** 77–84
34. Stains, J. P., and Gay, C. V. (2001) Inhibition of Na^+/Ca^{2+} exchange with KB-R7943 or bepridil diminished mineral deposition by osteoblasts. *J. Bone Miner. Res.* **16,** 1434–1443
35. Yang, H., Kim, A., David, T., Palmer, D., Jin, T., Tien, J., Huang, F., Cheng, T., Coughlin, S. R., Jan, Y. N., and Jan, L. Y. (2012) TMEM16F forms a Ca^{2+}-activated cation channel required for lipid scrambling in platelets during blood coagulation. *Cell* **151,** 111–122
36. Ladilov, Y., Haffner, S., Balser-Schäfer, C., Maxeiner, H., and Piper, H. M. (1999) Cardioprotective effects of KB-R7943: a novel inhibitor of the reverse mode of Na^+/Ca^{2+} exchanger. *Am. J. Physiol.* **276,** H1868–H1876
37. Bronckers, A., Kalogeraki, L., Jorna, H. J., Wilke, M., Bervoets, T. J., Lyaruu, D. M., Zandieh-Doulabi, B., Denbesten, P., and de Jonge, H. (2010) The cystic fibrosis transmembrane conductance regulator (CFTR) is expressed in maturation stage ameloblasts, odontoblasts and bone cells. *Bone* **46,** 1188–1196
38. Stalvey, M. S., and Clines, G. A. (2013) Cystic fibrosis-related bone disease: insights into a growing problem. *Curr. Opin. Endocrinol. Diabetes Obes.* **20,** 547–552
39. Le Henaff, C., Gimenez, A., Haÿ, E., Marty, C., Marie, P., and Jacquot, J.

(2012) The F508del mutation in cystic fibrosis transmembrane conductance regulator gene impacts bone formation. *Am. J. Pathol.* **180,** 2068–2075

40. Stalvey, M. S., Clines, K. L., Havasi, V., McKibbin, C. R., Dunn, L. K., Chung, W. J., and Clines, G. A. (2013) Osteoblast CFTR inactivation reduces differentiation and osteoprotegerin expression in a mouse model of cystic fibrosis-related bone disease. *PLoS ONE* **8,** e80098
41. Faria, D., Rock, J. R., Romao, A. M., Schweda, F., Bandulik, S., Witzgall, R., Schlatter, E., Heitzmann, D., Pavenstädt, H., Herrmann, E., Kunzelmann, K., and Schreiber, R. (2014) The calcium activated chloride channel Anoctamin 1 contributes to the regulation of renal function. *Kidney Int.* **85,** 1369–1381